Free Space Physical Optics Scattering by a Triangularly Meshed PEC Sphere Using Equivalent Point Dipoles

Abdullah Noor, Ramazan Daşbaşı*, Burak Polat
Department of Electronics and Communication Engineering, Yildiz Technical University, Istanbul, Turkey.

* Corresponding author. Tel.: 0212-358-5911; email: rdasbasi@yildiz.edu.tr
Manuscript submitted December 24, 2022; revised February 1, 2023; accepted March 14, 2023.
doi: 10.17706/ijapm.2023.13.4.53-61

Abstract: The success of the triangular meshing technique in plane wave scattering by perfect electric conductor bodies in free space is tested for the special case of a sphere under physical optics approximation by representing each facet as an equivalent electrical dipole source. The scattering patterns are observed to conform to the exact solution of the corresponding boundary value problem as well as CST™ simulation results.

Keywords: Computational electromagnetics, electromagnetic scattering, electromagnetic waves, physical optics, radar cross-section

1. Introduction

In the present work, we introduce an asymptotic analytical approach for electromagnetic scattering by Perfect Electric Conductor (PEC) surfaces defined by triangular facets in free space. The investigation starts with the derivation of the rotation dyadic of an arbitrarily oriented triangular facet and the equivalent moment of the electrical Hertzian dipole that characterizes the fields scattered by the PEC facet under homogeneous plane wave incidence and Physical Optics (PO) approximation [1], which is founded on Huygens-Fresnel principle derived originally from the Kirchhoff diffraction formula [2] introduced in 1883. The Principle of Superposition reveals the total fields scattered by arbitrarily shaped PEC surfaces. The performance of the method is tested for the canonical case of a PEC sphere w.r.t. exact expressions and CST Studio Suite™ (CST) [3] simulations of the scattered electrical field.

Time dependence $exp(-i\omega t)$ is assumed for phasor quantities. Here, $\omega = 2\pi f = 2\pi\frac{c_0}{\lambda} = kc_0$, where c_0 represents the speed of light in free space.

2. Formulation

2.1. Geometric Aspects of the Problem

Consider an arbitrarily oriented triangular facet S_F in global Cartesian $Ox_1x_2x_3$ −frame as illustrated in Fig. 1. It is defined by the position vectors of its vertices

$$\vec{r}_A = (x_{1A}, x_{2A}, x_{3A}),\ \vec{r}_B = (x_{1B}, x_{2B}, x_{3B}),\ \vec{r}_C = (x_{1C}, x_{2C}, x_{3C})$$

Let us denote the relative position vectors through the vertices by

$$\vec{r}_{AB} = \hat{x}_i(x_{iB} - x_{iA}),\ \vec{r}_{AC} = \hat{x}_i(x_{iC} - x_{iA})$$

Using summation convention. Their Euclidean norms are

$$|\vec{r}_{AB}| = [(x_{1B} - x_{1A})^2 + (x_{2B} - x_{2A})^2 + (x_{3B} - x_{3A})^2]^{\frac{1}{2}}$$

$$|\vec{r}_{AC}| = [(x_{1C} - x_{1A})^2 + (x_{2C} - x_{2A})^2 + (x_{3C} - x_{3A})^2]^{\frac{1}{2}}$$

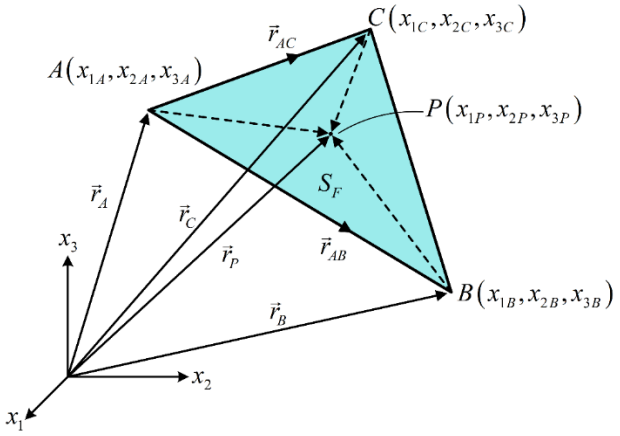

Fig. 1. Orientation of a triangular PEC facet S_F in global $Ox_1x_2x_3$ −frame.

We represent the associated unit vectors by

$$\hat{r}_{AB} = \hat{x}_i \frac{(x_{iB} - x_{iA})}{|\vec{r}_{AB}|},\ \hat{r}_{AC} = \hat{x}_i \frac{(x_{iC} - x_{iA})}{|\vec{r}_{AC}|}$$

The Eulerian transformation between the local Cartesian reference frame $Ox_1'x_2'x_3'$ and the global frame $Ox_1x_2x_3$ of the facet is defined as

$$\vec{r} = \bar{\bar{Q}} \cdot \vec{r}' + \vec{r}_A\ ,\ \hat{r} = \bar{\bar{Q}} \cdot \hat{r}' \text{ and } \vec{r}' = \bar{\bar{Q}}^T \cdot (\vec{r} - \vec{r}_A),\ \hat{r}' = \bar{\bar{Q}}^T \cdot \hat{r}$$

The rotation dyadic $\bar{\bar{Q}}$ has the typical properties $det\, \bar{\bar{Q}} = 1,\ \bar{\bar{Q}}^{-1} = \bar{\bar{Q}}^T$ with elements $Q_{ij} = \hat{x}_i \cdot \hat{x}_j'$. We specify the unit vectors of the local reference frame as

$$\hat{x}_1' \triangleq \hat{r}_{AB},\ \hat{x}_2' \triangleq \frac{[\hat{r}_{AC} - (\hat{r}_{AC} \cdot \hat{r}_{AB})\hat{r}_{AB}]}{|\hat{r}_{AC} - (\hat{r}_{AC} \cdot \hat{r}_{AB})\hat{r}_{AB}|}$$

$$\hat{x}_3' = \hat{x}_1' \times \hat{x}_2' = \frac{[\hat{r}_{AB} \times \hat{r}_{AC}]}{|\hat{r}_{AC} - (\hat{r}_{AC} \cdot \hat{r}_{AB})\hat{r}_{AB}|}$$

Then, the explicit expressions of the coordinates of vertices B and C in the local $Ox_1'x_2'$ −frame, as illustrated in Fig. 2, are given as

$$\begin{cases} x_{1B}' = Q_{11}(x_{1B} - x_{1A}) + Q_{21}(x_{2B} - x_{2A}) + Q_{31}(x_{3B} - x_{3A}) \\ x_{1C}' = Q_{11}(x_{1C} - x_{1A}) + Q_{21}(x_{2C} - x_{2A}) + Q_{31}(x_{3C} - x_{3A}) \\ x_{2C}' = Q_{12}(x_{1C} - x_{1A}) + Q_{22}(x_{2C} - x_{2A}) + Q_{32}(x_{3C} - x_{3A}) \end{cases}$$

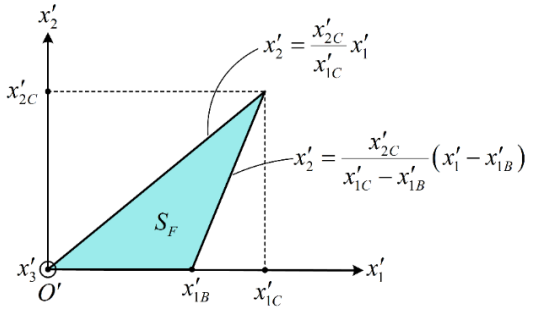

Fig. 2. Orientation of a triangular PEC facet in local $O'x_1'x_2'x_3'$ −frame.

2.2. Calculations of the Equivalent Point Dipoles

We consider a homogeneous monochromatic plane wave incidence in the direction

$$\hat{n}_{inc} = -\hat{x}_1 \sin\theta_{inc}\cos\phi_{inc} - \hat{x}_2 \sin\theta_{inc}\sin\phi_{inc} - \hat{x}_3\cos\theta_{inc} = \hat{x}_1 n_1 + \hat{x}_2 n_2 + \hat{x}_3 n_3$$

with fields

$$\begin{cases} \vec{E}_{inc} = \vec{E}_0\, exp(\,ik\hat{n}_{inc}\cdot\vec{r}) = \vec{E}_0\, exp(\,ik\hat{n}_{inc}\cdot\vec{r}_A)\, exp(\,ik\hat{n}_{inc}\cdot\bar{\bar{Q}}\cdot\vec{r}') \\ \vec{H}_{inc} = \vec{H}_0 e^{ik\hat{n}_{inc}\cdot\vec{r}} = \vec{H}_0\, exp(\,ik\hat{n}_{inc}\cdot\vec{r}_A)\, exp(\,ik\hat{n}_{inc}\cdot\bar{\bar{Q}}\cdot\vec{r}') \\ \vec{E}_0 = E_{\theta 0}\hat{\theta}(\theta_{inc},\phi_{inc}) + E_{\phi 0}\hat{\phi}(\phi_{inc}) \\ Z\vec{H}_0 = E_{\phi 0}\hat{\theta}(\theta_{inc},\phi_{inc}) - E_{\theta 0}\hat{\phi}(\phi_{inc}) \end{cases}$$

Here, $Z = \sqrt{\frac{\mu_0}{\varepsilon_0}}$ denotes the characteristic impedance of free space while

$$\begin{cases} \hat{\theta}(\theta_{inc},\phi_{inc}) = (\hat{x}_1\cos\phi_{inc} + \hat{x}_2\sin\phi_{inc})\cos\theta_{inc} - \hat{x}_3\sin\theta_{inc} \\ \hat{\phi}(\phi_{inc}) = -\hat{x}_1\sin\phi_{inc} + \hat{x}_2\cos\phi_{inc} \end{cases}$$

The (phasor) vector potential generated by the induction surface currents with density $\vec{J}_S$ are represented by the radiation integral

$$\vec{A}(\vec{r}) = \frac{\mu_0}{4\pi}\int_{S_F}\vec{J}_S(\vec{\xi})\frac{e^{ikR}}{R}\,dS,\ dS = dx_1' dx_2',\ R = |\vec{r} - \vec{\xi}| \tag{1a}$$

Under a first-order approximation its far-field shapes into

$$\vec{A}^{\text{ff}}(\vec{r}) \simeq \frac{\mu_0}{4\pi}\frac{e^{ikR_P}}{R_P}\int_{S_F}\vec{J}_S(\vec{\xi}_S)\,dS \tag{1b}$$

with $\vec{\xi}_S = \vec{\xi}\big|_{S_F}, \vec{r} - \vec{\xi}_S = \vec{r}'$, and $R_P = |\vec{r} - \vec{r}_P| = [(x_1 - x_{1P})^2 + (x_2 - x_{2P})^2 + (x_3 - x_{3P})^2]^{\frac{1}{2}}$. Here, we pick P as the central point of S_F defined by $\vec{r}_P = \frac{(\vec{r}_A + \vec{r}_B + \vec{r}_C)}{3}$.

We characterize the scattered far field (1b) by the far field of an electrical Hertzian dipole (HD) at $\vec{r} = \vec{r}_P$ having moment $\vec{p}$ as

$$\vec{A}^{HD}(\vec{r}) = \frac{\mu_0}{4\pi}(-i\omega\vec{p})\frac{e^{ikR_p}}{R_p} \tag{2a}$$

This requires

$$-i\omega\vec{p} = \int_{S_F}\vec{J}_S(\vec{\xi}_S)\,dS \tag{2b}$$

We set

$$\vec{J}_S(\vec{\xi}_S) = 2\hat{n}_F \times \vec{H}_{inc}\big|_{S_F} = \left(2\gamma_A\hat{n}_F \times \vec{H}_0\right) e^{ik\hat{n}_{inc}'\cdot\vec{r}'}\Big|_{x_3'=0}$$

with $\gamma_A \triangleq exp(\,ik\hat{n}_{inc}\cdot\vec{r}_A)$, $\hat{n}_F \triangleq \hat{x}_3'$ under PO approximation to get

$$-i\omega\vec{p} = \left(2\gamma_A\hat{n}_F \times \vec{H}_0\right)I,\ I = \int_{S_F} exp(\,ik\hat{n}_{inc}'\cdot\vec{r}_S')dx_1' dx_2'$$

The integral I is calculated by

$$I = \int_0^{x_{1C}'} exp(-ikn_1'x_1')\left[\int_0^{\frac{x_{2C}'}{x_{1C}'}x_1'} exp(-ikn_2'x_2')dx_2'\right]dx_1' - \int_{x_{1B}'}^{x_{1C}'} exp(-ikn_1'x_1')\left[\int_0^{\frac{x_{2C}'}{x_{1C}'-x_{1B}'}(x_1'-x_{1B}')} exp(-ikn_2'x_2')dx_2'\right]dx_1'$$

in a straightforward manner to get

$$\frac{k^2 I}{N_{BC}} = \begin{cases} \frac{i}{N_B N_C (N_B - N_C)} [N_C e^{-iN_B} \sin N_B - N_B e^{-iN_C} \sin N_C], N_B \neq N_C \neq 0 \\ -i \frac{e^{-iN_B}}{N_B^2} \sin N_B, N_B = N_C \neq 0 \\ i \frac{1}{N_C^2} [e^{-iN_C} \sin N_C - N_C], N_B = 0, N_C \neq 0 \\ i \frac{1}{N_B^2} [e^{-iN_B} \sin N_B - N_B], N_B \neq 0, N_C = 0 \\ 1, N_B = N_C = 0 \end{cases}$$

with the definitions

$$2N_B \triangleq k n_1' x_{1B}',\ 2N_C \triangleq k(n_2' x_{2C}' + n_1' x_{1C}'),\ 2N_{BC} \triangleq k^2 x_{1B}' x_{2C}'$$

2.3. Explicit Expression of the Electrical Field of an Equivalent Point Dipole

The electrical field associated with the vector potential Eq. (2) can be expressed by

$$\vec{E}^{HD}(\vec{r}) = \omega^2 \mu_0 \bar{\bar{G}}(\vec{r}, \vec{r}_P) \cdot \vec{p} = 2i\omega\mu_0 I \gamma_A \bar{\bar{G}}(\vec{r}, \vec{r}_P) \cdot (\hat{n}_F \times \vec{H}_0)$$

Here, $\bar{\bar{G}} = \hat{x}_j \hat{x}_n g_j^n$ is the Green's dyadic of free space with g_j^n $j, n = 1,2,3$ representing the x_j −axis electrical field component at $\vec{r} = (x_1, x_2, x_3)$ generated by the Hertzian dipole (with unit moment) located at $\vec{r}_P = (x_{1P}, x_{2P}, x_{3P})$ and directed along (positive) x_n −axis. They are given by

$$g_i^i = \frac{e^{ikR_P}}{4\pi R_P}\left[\xi_1 - \frac{(x_i - x_{iP})^2}{R_P^2}\xi_2\right],\ i = 1,2,3, \quad g_2^1 = -\frac{(x_1 - x_{1P})(x_2 - x_{2P})}{R_P^2}\frac{e^{ikR_P}}{4\pi R_P}\xi_2 = -g_1^2,$$
$$g_3^2 = -\frac{(x_2 - x_{2P})(x_3 - x_{3P})}{R_P^2}\frac{e^{ikR_P}}{4\pi R_P}\xi_2 = g_2^3, \quad g_1^3 = -\frac{(x_1 - x_{1P})(x_3 - x_{3P})}{R_P^2}\frac{e^{ikR_P}}{4\pi R_P}\xi_2 = g_3^1,$$

where $\xi_1 = 1 - \frac{1}{ikR_P} - \frac{1}{k^2 R_P^2}$, $\xi_2 = 1 - \frac{3}{ikR_P} - \frac{3}{k^2 R_P^2}$.

Straightforward calculations reveal the components of the PO electrical field of the facet $\vec{E}^{PO}(\vec{r}) = \hat{x}_1 E_1 + \hat{x}_2 E_2 + \hat{x}_3 E_3$ as

$$E_j = 2ikI\gamma_A \frac{1}{|\vec{r}_{AB}||\vec{r}_{AC}|} \frac{1}{|\hat{r}_{AC} - (\hat{r}_{AC} \cdot \hat{r}_{AB})\hat{r}_{AB}|} \times \left[\gamma_{AB} \sum_{n=1}^{3} g_j^n (x_{nC} - x_{nA}) - \gamma_{AC} \sum_{n=1}^{3} g_j^n (x_{nB} - x_{nA})\right] \quad (3)$$

where we define

$$\gamma_{AB} \triangleq (x_{1B} - x_{1A})\left[E_{\phi 0} \cos\phi_{inc} \cos\theta_{inc} + E_{\theta 0} \sin\phi_{inc}\right] + (x_{2B} - x_{2A})\left[E_{\phi 0} \sin\phi_{inc} \cos\theta_{inc} - E_{\theta 0} \cos\phi_{inc}\right]$$
$$- (x_{3B} - x_{3A}) E_{\phi 0} \sin\theta_{inc}$$

$$\gamma_{AC} \triangleq (x_{1C} - x_{1A})\left[E_{\phi 0} \cos\phi_{inc} \cos\theta_{inc} + E_{\theta 0} \sin\phi_{inc}\right] + (x_{2C} - x_{2A})\left[E_{\phi 0} \sin\phi_{inc} \cos\theta_{inc} - E_{\theta 0} \cos\phi_{inc}\right]$$
$$- (x_{3C} - x_{3A}) E_{\phi 0} \sin\theta_{inc}$$

2.4. Total Scattered Electrical Far Field due to Equivalent Point Dipoles

The far field approximation can be incorporated as

$$(x_1 - x_{1P}) \to x_1 = r \sin\theta \cos\phi, \quad (x_2 - x_{2P}) \to x_2 = r \sin\theta \sin\phi,\ (x_3 - x_{3P}) \to x_3 = r \cos\theta,\ R_P \to r,\ \xi_1 \to$$
$$1 - \frac{1}{ikr} - \frac{1}{k^2 r^2},\ \xi_2 \to 1 - \frac{3}{ikr} - \frac{3}{k^2 r^2},\ e^{ikR_P} \to \gamma_P e^{ikr}$$

with the definition

$$\gamma_P \triangleq exp(-ik\hat{r} \cdot \vec{r}_P) = exp[-ik(x_{1P} \sin\theta \cos\phi + x_{2P} \sin\theta \sin\phi + x_{3P} \cos\theta)].$$

This shapes the dyadic components into $g_j^n = \frac{e^{ikr}}{4\pi r} \gamma_P \Delta_j^n$ with

$$\Delta_1^1 = \xi_1 - \xi_2 \sin^2\theta \cos^2\phi, \quad \Delta_2^2 = \xi_1 - \xi_2 \sin^2\theta \sin^2\phi, \quad \Delta_3^3 = \xi_1 - \xi_2 \cos^2\theta\ \Delta_2^1 = -\xi_2 \sin^2\theta \cos\phi \sin\phi = -\Delta_2^1,$$
$$\Delta_1^3 = -\xi_2 \sin\theta \cos\theta \cos\phi = \Delta_3^1, \quad \Delta_3^2 = -\xi_2 \sin\theta \cos\theta \sin\phi = \Delta_2^3$$

and one substitutes them into Eq. (3) to get

$$E_j = 2ikI \frac{1}{|\vec{r}_{AB}||\vec{r}_{AC}|} \frac{1}{|\hat{r}_{AC}-(\hat{r}_{AC}\cdot\hat{r}_{AB})\hat{r}_{AB}|} \gamma_A\gamma_P \frac{e^{ikr}}{4\pi r} \sum_{n=1}^{3} \Delta_j^n [\gamma_{AB}(x_{nC}-x_{nA}) - \gamma_{AC}(x_{nB}-x_{nA})] \quad (4)$$

The $\theta-$ and $\phi-$components of the total scattered electrical field vector can be synthesized in terms of the Cartesian components Eq. (4) over the illuminated facets $(\hat{n}_{inc}\cdot\hat{n}_F < 0)$ as

$$E_{\theta,\phi}^{PO} = \frac{e^{ikr}}{kr} \sum_{\substack{\text{Illuminated} \\ \text{facets}}} f_{\theta,\phi}(\theta,\phi; k\vec{r}_A, k\vec{r}_B, k\vec{r}_C) \quad (5)$$

with (electrically normalized) scattering patterns

$$f_\theta = \frac{ik^2 I}{2\pi} \frac{1}{|\vec{r}_{AB}||\vec{r}_{AC}|} \frac{1}{|\hat{r}_{AC}-(\hat{r}_{AC}\cdot\hat{r}_{AB})\hat{r}_{AB}|} \gamma_A\gamma_P \sum_{n=1}^{3} \begin{Bmatrix} [\cos\theta\cos\phi\,\Delta_1^n + \cos\theta\sin\phi\,\Delta_2^n - \sin\theta\,\Delta_3^n] \\ \times [\gamma_{AB}(x_{nC}-x_{nA}) - \gamma_{AC}(x_{nB}-x_{nA})] \end{Bmatrix} \quad (6a)$$

$$f_\phi = \frac{ik^2 I}{2\pi} \frac{1}{|\vec{r}_{AB}||\vec{r}_{AC}|} \frac{1}{|\hat{r}_{AC}-(\hat{r}_{AC}\cdot\hat{r}_{AB})\hat{r}_{AB}|} \gamma_A\gamma_P \sum_{n=1}^{3} \begin{Bmatrix} [-\sin\phi\;\;\Delta_1^n + \cos\phi\;\;\Delta_2^n] \\ \times [\gamma_{AB}(x_{nC}-x_{nA}) - \gamma_{AC}(x_{nB}-x_{nA})] \end{Bmatrix} \quad (6b)$$

3. Numerical Implementations

3.1. The Exact Expression of the Scattered Electrical Field

We shall test the performance of the current PO formulation by comparing to exact scattered electrical fields for a PEC illustrated in Fig. 3 and simulations by CST™.

We consider an incidence as $\hat{n}_{inc} = -\hat{x}_3,\ \vec{E}_{inc} = \hat{x}_1\, exp(-ikx_3)$ under which the exact scattered fields are already available in [4] as

$$\vec{E}^{exact} = \hat{\theta}E_\theta^{exact} + \hat{\phi}E_\phi^{exact} = \frac{e^{ikr}}{kr}\left[\hat{\theta}f_\theta^{exact}(\theta,\phi) + \hat{\phi}f_\phi^{exact}(\theta,\phi)\right]$$

$$f_\theta^{exact}(\theta,\phi) = S_1(\theta)\cos\phi\,, \qquad f_\phi^{exact}(\theta,\phi) = -S_2(\theta)\sin\phi$$

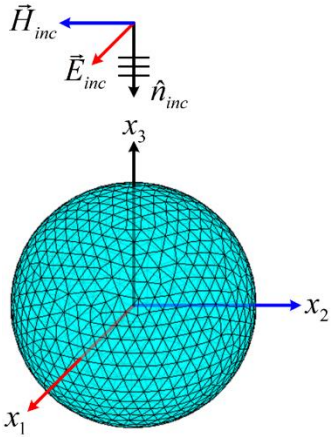

Fig. 3. Homogeneous plane wave incidence on a PEC sphere centered at the origin of the global $Ox_1x_2x_3$ −frame.

$$S_1(\theta) = \sum_{n=1}^{\infty} (-i)^{n+1} \left[A_n \frac{P_n^1(\cos\theta)}{\sin\theta} + iB_n \frac{d}{d\theta} P_n^1(\cos\theta) \right]$$

$$S_2(\theta) = \sum_{n=1}^{\infty} (-i)^{n+1} \left[A_n \frac{d}{d\theta} P_n^1(\cos\theta) + iB_n \frac{P_n^1(\cos\theta)}{\sin\theta} \right]$$

$$A_n = -(-i)^n \frac{2n+1}{n(n+1)} \frac{j_n(ka)}{h_n^{(1)}(ka)}, \qquad B_n = (-i)^{n+1} \frac{2n+1}{n(n+1)} \frac{\frac{d}{d(ka)}[ka\, j_n(ka)]}{\frac{d}{d(ka)}[ka\, h_n^{(1)}(ka)]}$$

Here, a is the radius of the sphere; j_n and $h_n^{(1)}$ are spherical Bessel and Hankel functions (of the first kind) of order n and P_n^1 is the associated Legendre polynomial of degree n and order 1. Their numerical calculations are performed in MATLAB™ based on the formulas tabulated in [5].

3.2. Physical Optics vs. Exact and Simulation Results

In Fig. 4 PO, exact analytical and CST™ simulation data are provided on E −plane (i.e., on Ox_1x_3 −plane) in the angular range

$$\theta \in [0^o, 180^o], \phi = 0^o \cup \theta \in [0^o, 180^o], \phi = 180^o$$

for (range and amplitude normalized) total scattered electrical fields

$$\begin{cases} 20\,log_{10}|kr \cdot E_\theta^{PO}| = 20\,log_{10}\,|\sum_{\text{Illuminated facets}} f_\theta\,| \\ 20\,log_{10}|kr \cdot E_\theta^{exact}| = 20\,log_{10}|f_\theta^{exact}(\theta,\phi)| = 20\,log_{10}|S_1(\theta)\,cos\,\phi| \\ 20\,log_{10}|kr \cdot E_\theta^{CST}| \end{cases}$$

Forward scattering is intensified and shapes into a pencil beam with increasing electrical radius ka. We observe that exact analytical and CST™ results fit well for all ka values, while their discrepancy with PO formulation over the sidelobes diminishes for increasing values of ka, as required theoretically.

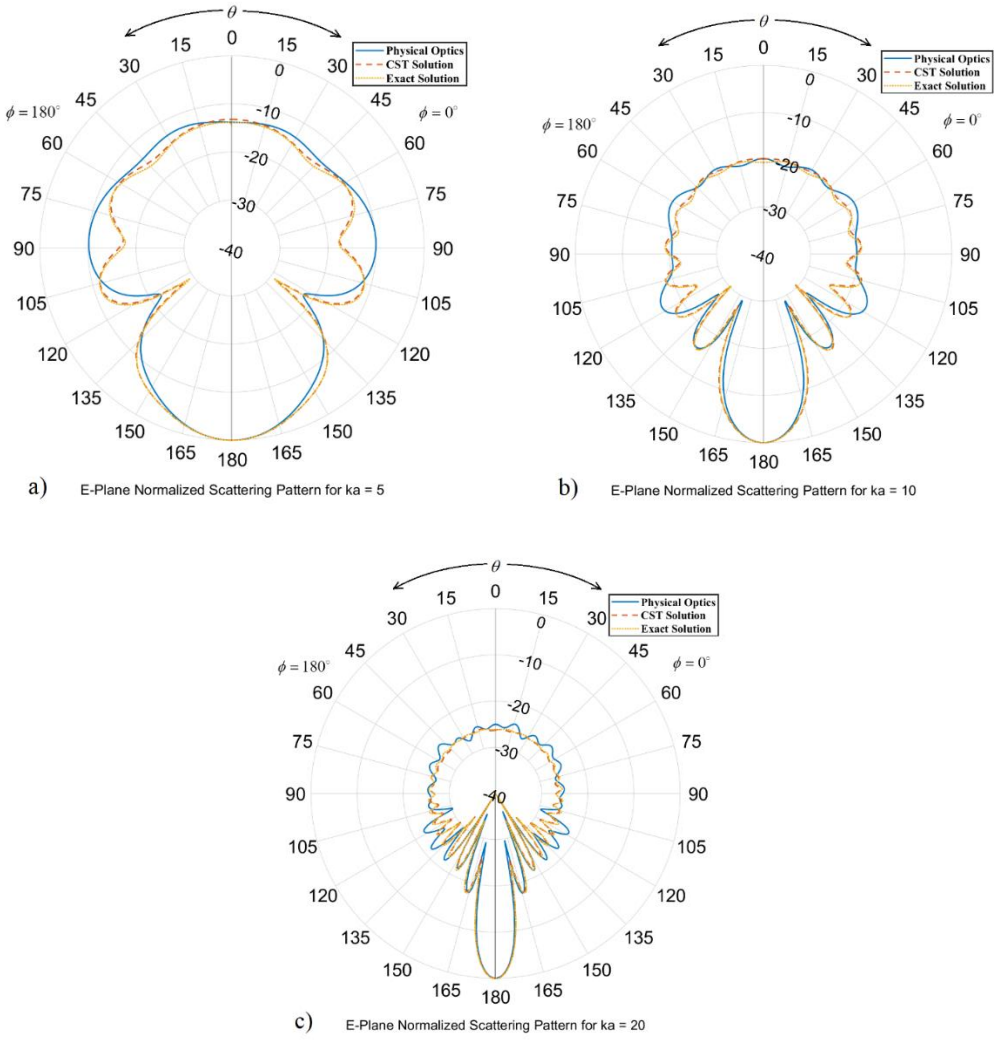

Fig. 4. E −plane normalized scattering patterns for a) $ka = 5$[rad], b) $ka = 10$[rad], c) $ka = 20$[rad].

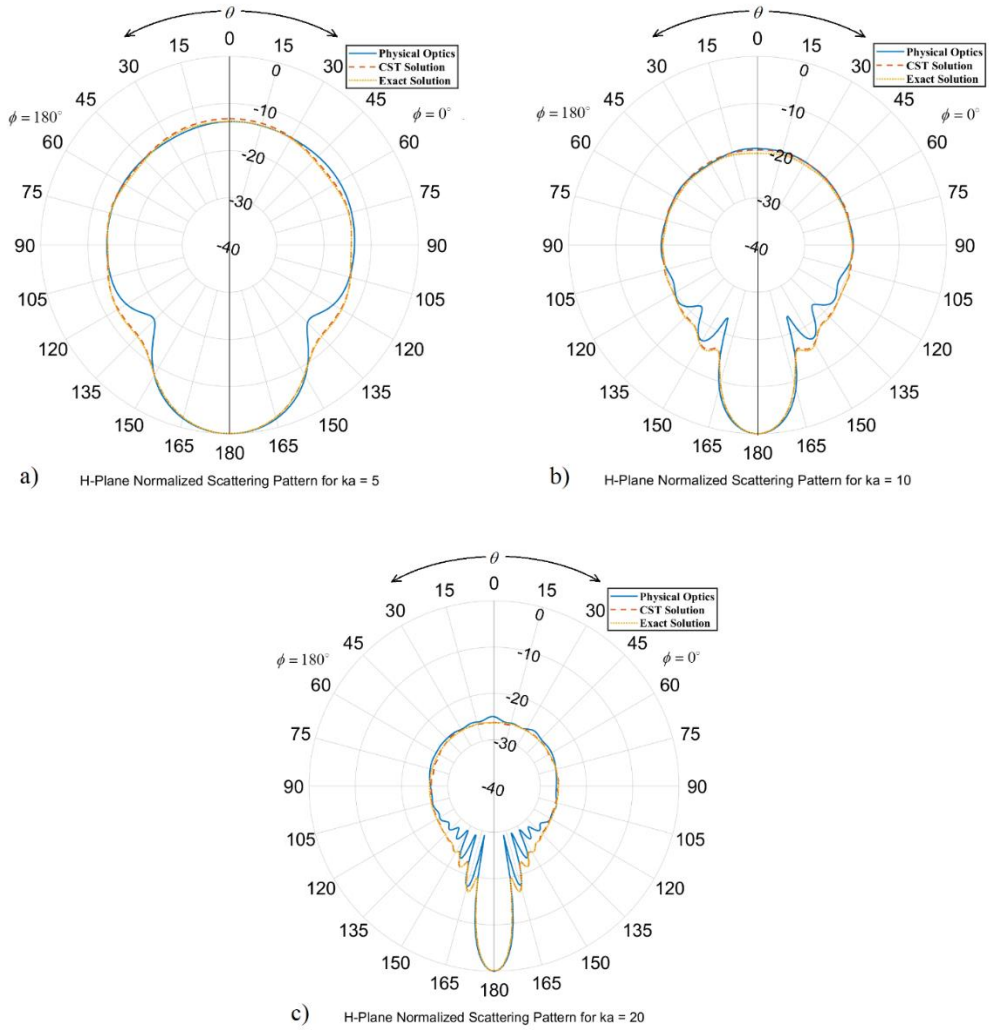

Fig. 5. H −plane normalized scattering patterns for a) $ka = 5$[rad], b) $ka = 10$[rad], c) $ka = 20$[rad].

A similar implementation carried out on H −plane (i.e., on Ox_2x_3 −plane) in the angular range

$$\theta \in [0^o, 180^o], \phi = 90^o \cup \theta \in [0^o, 180^o], \phi = -90^o$$

for ϕ −components of the total scattered electrical fields

$$\begin{cases} 20\,log_{10}\left|kr \cdot E_{\phi}^{PO}\right| = 20\,log_{10}\left|\sum_{\text{Illuminated facets}} f_{\phi}\right| \\ 20\,log_{10}\left|kr \cdot E_{\phi}^{exact}\right| = 20\,log_{10}\left|f_{\phi}^{exact}(\theta,\phi)\right| = 20\,log_{10}|S_2(\theta)\,sin\,\phi| \\ 20\,log_{10}\left|kr \cdot E_{\phi}^{CST}\right| \end{cases}$$

Fig. 5 reveals similar observations. Picking the dimensions of the facets around 0.15λ is observed to optimize numerical convergence in triangular meshing. The axial symmetry in the scattering patterns is a feature of the rotational symmetry of the scatterer.

4. Concluding Remarks

The high accuracy obtained in the numerical results for the canonical case of a PEC sphere reveals the success of representing each facet in a triangularly meshed PEC surface by an equivalent electrical Hertzian dipole. We observe that the requirements on the minimum electrical size of the scatterer for the

convergence of the present PO formulation are already satisfied fully in microwave bands in relation to RCS predictions of aircrafts and naval vessels. The presented analytical-asymptotic method has a significant computational advantage when compared to the approaches (such as in [6, 7]) which compute the double integral I numerically. The equivalent Hertzian electrical dipoles also provide the formulation to be extendable to complex media by employing the associated Green's dyadic $\bar{\bar{G}}(\vec{r},\vec{r}_P)$ in virtue of the Directional Currents Method devised in [8, 9].

The present formulation is planned to be extended to PEC and impedance bodies located over a lossy dielectric half-space using the Green's dyadic available already in [10]. Of special interest is the test of the performance of the present PO formulation for PEC surfaces with tips and edges such as plates, wedges, cones, and rectangular boxes in simulating 3-D platforms which may require incorporating higher order PO terms or the modified theory of PO [11] that involves edge contributions to the total scattered fields.

Conflict of Interest

The authors declare no conflict of interest.

Author Contributions

Burak Polat provided the analytical formulation, Abdullah Noor and Ramazan Daşbaşı developed algorithmic flow, implemented software codes, and performed numerical analyses. All authors approve the final version.

Funding

This work was supported by Research Fund of the Yildiz Technical University. Project Number: FBA-2021-4310.

References

[1] Pathak, P. H. & Burkholder, R. J. (2022). *Electromagnetic Radiation, Scattering and Diffraction*. IEEE Press, Wiley.

[2] Kirchhoff, G. (1883). On the theory of light rays. *Annals of Physics, 254(4)*, 663–695. https://doi.org/10.1002/andp.18832540409 (in German)

[3] CST Studio Suite. Electromagnetic simulation software. Retrieved from https://www.3ds.com/products-services/simulia/products/cst-studio-suite/

[4] Ruck, G. T., Barrick, D. E, Stuart, W. D., & Kirchbaum, C. K. (1970). *Radar Cross Section Handbook*. New York Kluwer Academic/Plenum Publishers

[5] Abramowitz, M. & Stegun, I. A. (1974). *Handbook of Mathematical Functions with Formulas, Graphs, and Mathematical Table*s, Dover Publications.

[6] Garrido, E. E. (2000). *Graphical User Interface for a Physical Optics Radar cross Section Prediction Code*. Monterey, CA: Naval Postgraduate School.

[7] Noor, A., Daşbaşı, R., & Polat, B. (2022). Physical optics Scattering by a PEC missile in uniform rectilinear motion. *The European Journal of Research and Development*, *2(2)*, 421–428. doi:10.56038/ejrnd.v2i2.88

[8] Polat, B., & Daşbaşı, R. (2020). Hertzian dipoles supporting directional currents. *Proceedings of the 2020 IEEE Ukrainian Microwave Week (UkrMW)* (pp. 494–500). doi: 10.1109/UkrMW49653.2020.9252718

[9] Polat, B., & Daşbaşı, R. (2021). Analysis of conical horn antenna radiation over ground by directional currents method. *Proceedings of the 2021 20th International Conference on Microwave Techniques*

(COMITE) (pp. 1–6). doi: 10.1109/COMITE52242.2021.9419878

[10] Polat, B., & Daşbaşı, R. (2020). Physical optics scattering by a PEC plate located vertically over a dielectric half-space. *Progress In Electromagnetics Research B, 88*, 151–173. doi:10.2528/PIERB20052802

[11] Umul, Y. Z. (2009). Improved equivalent source theory, *Journal of the Optical Society of America A, 26(8)*, 1798–180. doi:10.1364/JOSAA.26.001798